Analysis on Thermal Islands Effectors in Ramadi City, Iraq Using Multi-temporal Landsat Images

Assoc. Prof. Dr.Ismael Abbas Hurat
unversity of anbar
educatin college for women
Department of geography
Ismael.abbass@uoanbar.edu.iq

Abstract

This paper analyzes the effects of urban density, vegetation cover, and water body on thermal islands measured by land surface temperature in Al Anbar province, Iraq using multi-temporal Landsat images. Images from Landsat 7 ETM and Landsat 8 OLI for the years 2000, 2014, and 2018 were collected, pre-processed, and anal yzed. The results suggested that the strongest correlation was found between the Normalized Difference Built-up Index (NDBI) and the surface temperature. The correlation between the Normalized Difference Vegetation Index (NDVI) and the surface temperature was slightly weaker compared to that of NDBI. However, the weakest correlation was found between the Normalized Difference Water Index (NDWI) and the temperature. The results obtained in this research may help the decision makers to take actions to reduce the effects of thermal islands by looking at the details in the produced maps and the analyzed values of these spectral indices.

Keywords: Thermal Islands, Landsat, Spectral Indices, Remote Sensing, GIS

1. Introduction

Climate change possesses significant short and long terms threats to urban cities and their developments (Comarazamy, Gonzalez, & Luvall, 2015). Therefore, climatological factors such as land surface temperature is often used in urban studies (Alexander, O'Dwyer, Brennan, Mills, & Lynch, 2017). Land surface temperature (LST) is a good indicator of the energy balance at Earth's surface because it is one key parameter in the physics of land surface processes on both regional and global scales (Centre for Geoinformatics & Planetary Studies, Dept. of Geology, Periyar University, Salem, Tamilnadu, India, S., C.R., & Centre for Geoinformatics & Planetary Studies, Dept. of Geology, Periyar University, Salem, Tamilnadu, India, 2016). LST combines the results of surface-atmosphere interactions and energy fluxes between the atmosphere and the ground. Therefore, LST measurements are required for a wide variety of climatic, hydrologic, ecological, and biogeochemical studies. Temperature influences weather and climate

patterns control the life of food crops (Morrow, Huggins, & Reganold, 2017).

Remote sensing provides satellite or aerial imagery that can be used to generate many forms of spatial information such as urban areas, land use types, vegetated areas, water bodies and other information about utilities and infrastructures in a region (He, Gao, Huang, Ma, & Dou, 2017). On the other hand, GIS provides efficient and useful solutions for creating, storing, analyzing and visualizing those data acquired using remote sensing.

The advancement of these technologies has improved the research of analyzing the impacts of thermal islands on urbanization, vegetation cover, and water bodies. Remote sensing developed in the last decades providing sensors capturing satellite images of land, which represent with a high scale of resolution of the objects on the surface of the Earth. This representation is of great importance to planners and land managers, where a wide range of imaging scales are operating. For example, freely available Landsat images over a considerable period, from the 1970s onwards provide great information help in analyzing the thermal island effectors (Zhu, Woodcock, Holden, & Yang, 2015).

The main goal of this research is to detect the impacts of thermal islands on three main variables including urban areas, vegetated lands, and water bodies. The specific objectives are (1) calculating three spectral indices that represent urban density (NDBI, Normalized Difference Building Index), vegetation cover (NDVI, Normalized Difference Vegetation Index), and water bodies (NDWI, Normalized Difference Water Index), (2) calculating the land surface temperature (LST), and (3) analyzing the correlation between the spectral indices and the LST over different grids in the area of interest.

2. Materials and Methods

This section explains the materials including the study area and datasets, and the proposed methodology.

2.1 Study Area and Datasets

2.1.1 Study Area

The study area of this research is Al Anbar Governorate, or Anbar Province (**Figure 1**). It is the largest governorate in Iraq by area. Encompassing much of the country's western territory, it shares borders with Syria, Jordan, and Saudi Arabia. The provincial capital is Ramadi; other important cities include Fallujah and Haditha. The population of Al Anbar in 2017 is estimated to be about 1,500,000.

Geographically, Anbar governorate is considered part of the Arabian Peninsula. The region's geography is a combination of steppe around the Euphrates river and true desert, characterized by a desert climate, low rainfall and a large variation in temperature between day

and night. Summer temperatures rise to 42 degrees Celsius, whilst in the winter average lows reach 9 degrees Celsius. The northwesterly and southwesterly winds are sometimes to a maximum speed of 21 m/s. Average rainfall in winter to 115 mm.

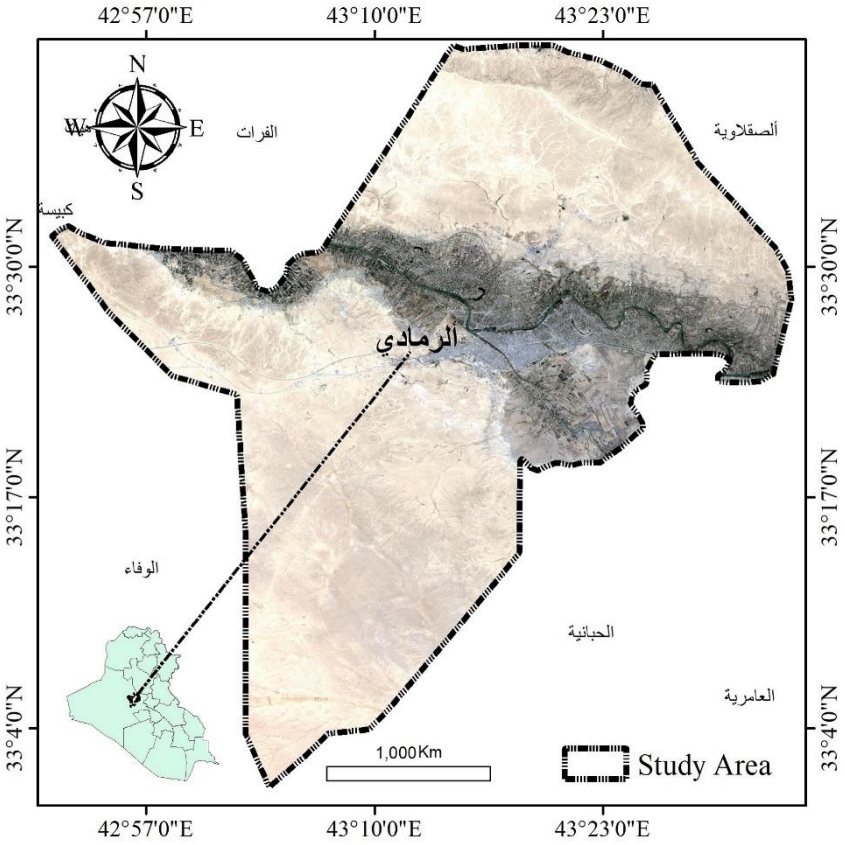

Figure 1: Geographic location of the study area (Ramadi City, Iraq).

2.1.2 Datasets

In this study, few Landsat images were acquired from the USGS website (**Figure 2**). **Table 1** shows the Landsat image series collected for the study area to extract the spectral indices and the LST information. Overall, three images were acquired which cover the study area. The acquisition date of the images ranged from 22 August 2000 to 16 August 2018. In addition, the highest cloud cover was 5% expected to be non-problematic for the spectral indices and the LST extraction in the study area.

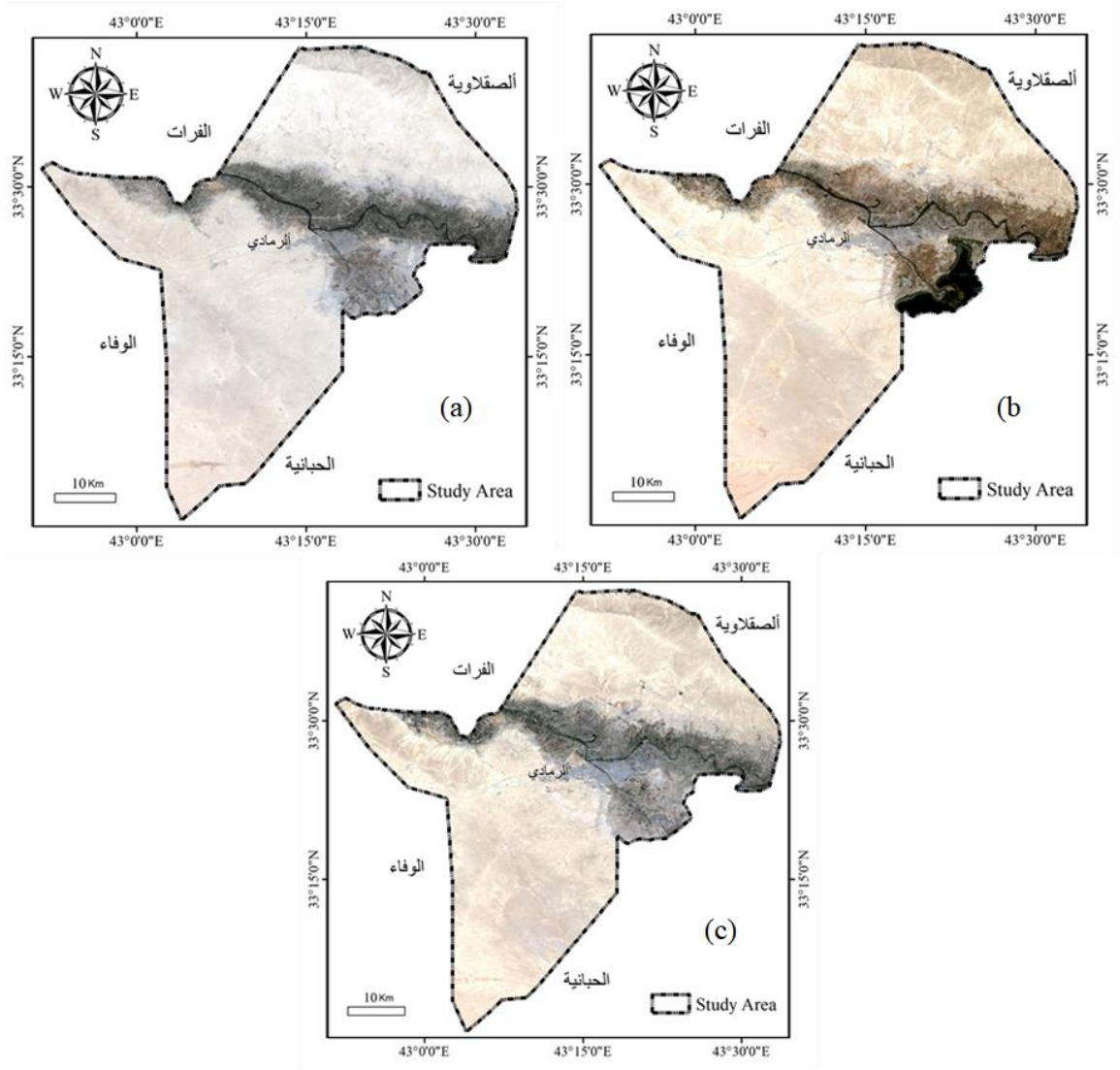

Figure 2: The Landsat base maps of the study area for the year (a) 2000, (b) 2014, and (c) 2018.

Table 1: Landsat images and their characteristics used in this research.

Dataset	Acquisition Date	Path	Raw	Cloud Cover	Sensor
Image 1	2000-08-22	169	37	0	LANDSAT_7 ETM
Image 2	2014-08-21	169	37	5%	LANDSAT 8 OLI
Image 3	2018-08-16	169	37	0	LANDSAT 8 OLI

2.2 Proposed Methodology

2.2.1 Flowchart of Methodology

Figure 3 shows the overall workflow applied in this research to find out what affects the land surface temperature from urbanization, vegetation cover, or water extents over the investigated three dates, 2000, 2014, and 2018. It started by data collection from USGS

website available online for free. Three Landsat images were collected for the study area. One image was based on the Landsat 7 ETM sensor with 7 spectral bands including a thermal band. While the other two images were based on the Landsat 8 OLI sensor with 11 spectral bands including two thermal bands. The three datasets were pre-processed to reduce the malfunction error effects and reduce the systematic noise by radiometric calibration, atmospheric correction, geometric correction, and spatial subset to reduce the computational need by clipping the scene only to cover the study area. The analysis was performed in two main steps including the calculation of three spectral indices namely NDBI, NDVI, and NDWI, and the calculation of the LST. Then, the correlation between the spectral indices and the LST was analyzed by GIS visualization and scatter plots. The details of each step is presented in the next sections.

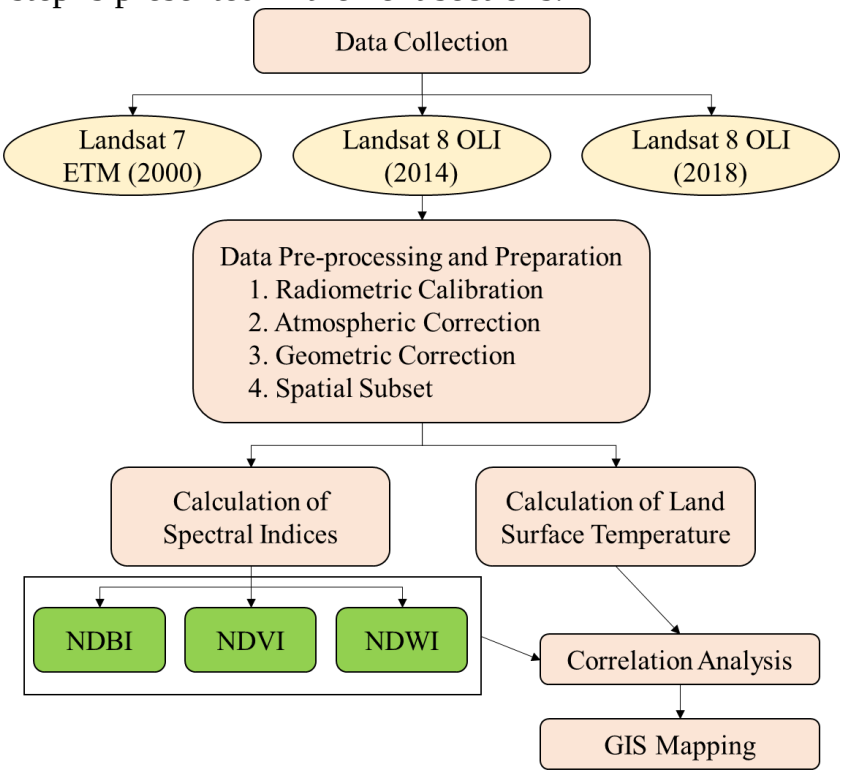

Figure 3: Flowchart of the proposed methodology in this research.

2.2.2 Image Pre-processing

Since the pre-processing is crucial for making the acquired images by remote sensing technologies ready for analysis (Lavender & Lavender, 2015), this study has applied several preprocessing steps on the Landsat 7 ETM and 8 OLI images before the analysis. Those steps consisted of radiometric calibration, geometric correction, atmospheric correction, and spatial subset. They helped to reduce the malfunction errors and reduce the noise from the images. It also helped to co-register the images correctly and remove the sunlight effects from the images. The images were also standardized the pixel values (from 0 to 1) that simplified the classification process. In the

first step-radiometric calibration, the digital numbers of the raw images were converted into radiance values (radiometric calibration) using the gain and offset values retrieved from the metadata file of the data. Second, the radiance values were normalized and converted into surface reflectance. This step was crucial as it helped to remove the variations due to atmospheric conditions and the bi-directional reflectance distribution function (BRDF) (Zhang, Bai, Wu, & Gong, 2016; Hilker, 2018). After that, the images were geometrically corrected and co-registered to ensure coincident with each other and the ground truth data, which were collected from Google Earth. Finally, the QUAC atmospheric correction algorithm was used to convert the radiance to reflectance and retrieve the spectral reflectance of the image (Bernardo, Watanabe, Rodrigues, & Alcântara, 2017). Finally, the images were subset to cover only the area of interest.

2.2.3 Calculation of Spectral Indices

NDVI is robust, empirical measures of vegetation activity at the land surface. They enhance the vegetation signal from measured spectral responses by combining two (or more) different wavebands, often in the red (0.6-0.7 mm) and near-infrared wavelengths (0.7-1.1 mm). Reflected red energy decreases with plant development due to chlorophyll absorption within actively photosynthetic leaves. Reflected near-infrared energy will increase with plant development through scattering processes (reflection and transmission) in healthy, turgid leaves. The NDVI is calculated using the **Equation 1**.

In contrast, NDBI provides coverage for a range of land cover types. It is useful for quantifying change in multitemporal images. It is calculated using the **Equation 2**. Moreover, NDWI proposed by McFeeters is designed to: (1) maximize the reflectance of the water body in the green band; (2) minimize the reflectance of water body in the NIR band. McFeeters's NDWI is calculated as presented in **Equation 3**.

$$NDVI = \frac{\rho NIR - \rho RED}{\rho NIR + \rho RED} \quad (1)$$

$$NDBI = \frac{\rho SWIR - \sigma NIR}{\rho SWIR + \sigma NIR} \quad (2)$$

$$NDWI = \frac{\rho Green - \rho NIR}{\rho Green + \rho NIR} \quad (3)$$

2.2.4 Calculation of LST

To calculate LST from Landsat images, thermal bands were used. For Landsat 7 ETM, Band 6 - Thermal Infrared (10.40 - 12.50) was used. However, For Landsat 8 OLI, Band 10 (10.60 – 11.19) was used. These bands were used to derive brightness temperature. This was done in three steps. First, the radiance values were converted into Top of Atmosphere Radiance. Then, the result was used to create the

temperature raster in degrees kelvin. Finally, the temperature unit was converted from kelvin into Celsius.

3. Results and Discussions

All indices applied in this study, including NDVI, NDBI, and NDWI, were extracted from the Landsat 7 ETM and Landsat-8 OLI images. **Figure 4** shows the NDVI maps produced for the study area in 2000, 2014, and 2018. The NDVI maps provide consistent, spatial and temporal comparisons of vegetation conditions. These maps are useful to monitor Earth's terrestrial photosynthetic vegetation activity to support phonologic research, change detection, and biophysical interpretations. In addition, urban areas are raising all over the world and in many countries, people are migrating from rural areas into more vibrant cities for better education and financial developments. This issue has affected many sectors including environment, agriculture, and transportation. This research investigated the correlation between the urban density (indicated by NBDI) and the LST over three periods, 2000, 2014, and 2018. The NDBI maps are shown in **Figure 5**. Moreover, water body mapping approaches have been developed to extract water bodies from Landsat images. The water body map is shown in **Figure 6,** extracted by the NDWI.

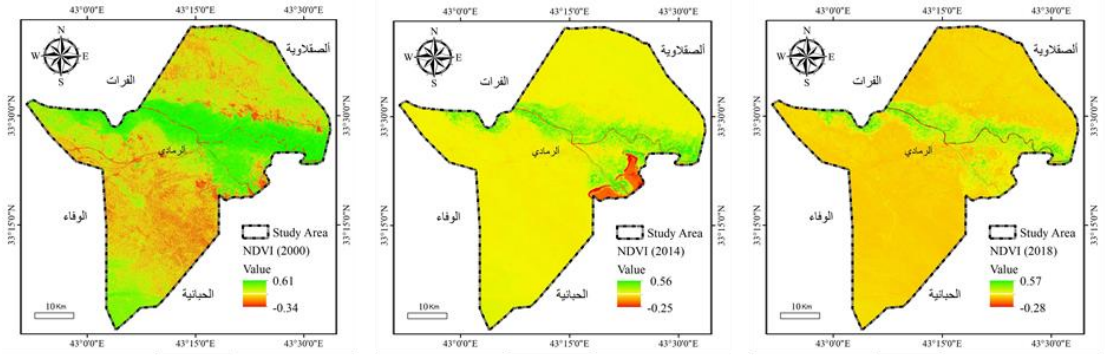

Figure 4: The Landsat base maps of the study area for the year (a) 2000, (b) 2014, and (c) 2018.

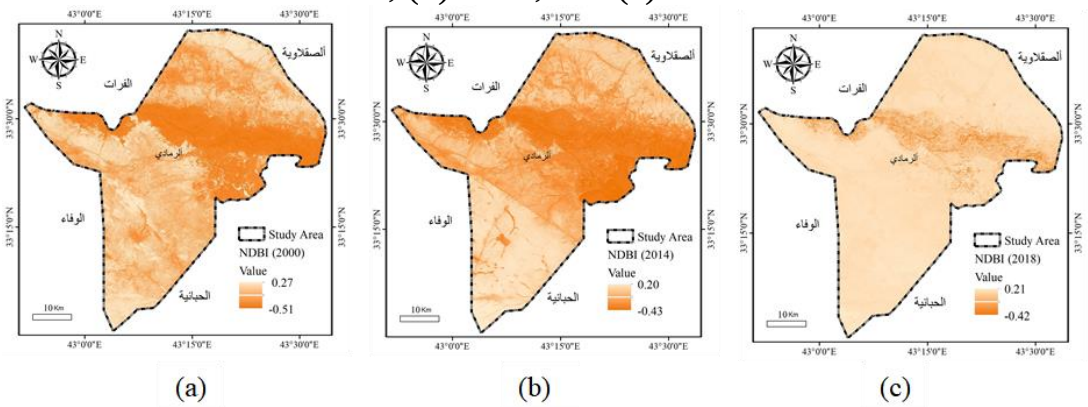

Figure 5: The Landsat base maps of the study area for the year (a) 2000, (b) 2014, and (c) 2018.

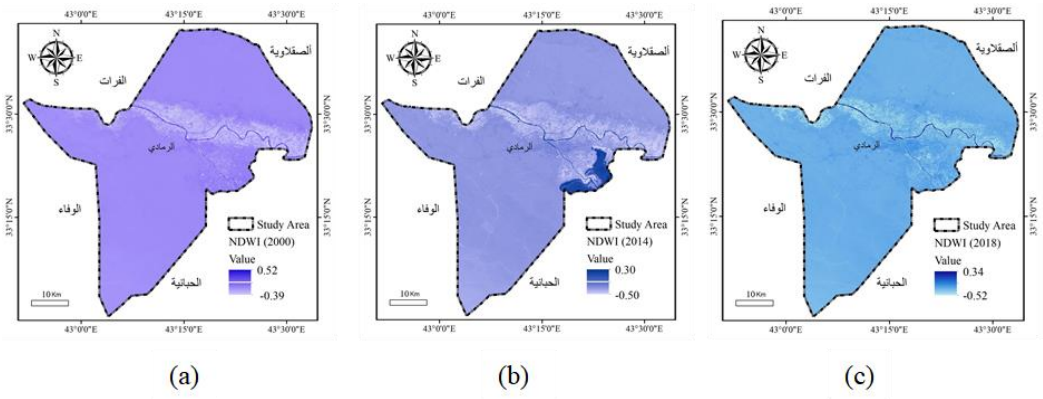

Figure 6: The Landsat base maps of the study area for the year (a) 2000, (b) 2014, and (c) 2018.

3.4 Results of LST

Figure 7 shows the LST maps produced for the study area using Landsat images in 2000, 2014, and 2018. The LST in 2000, suggests that the lowest and highest temperature were about 22 ℃ and 50 ℃, respectively. In 2014, the lowest temperature was 26 and the highest read was 50℃. The temperature even went up as measured in 2018. The lowest and highest temperature values in this year was 27 ℃ and 53 ℃, respectively.

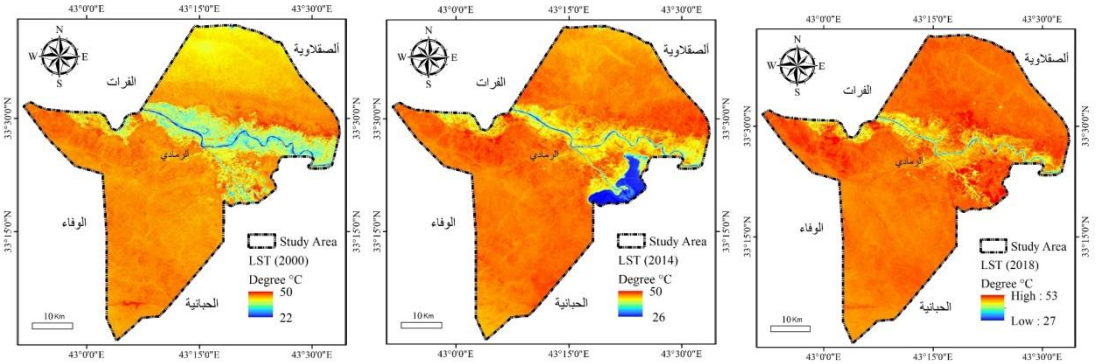

Figure 7: The Landsat base maps of the study area for the year (a) 2000, (b) 2014, and (c) 2018.

3.5 Results of Correlation Analysis between Thermal Island Effectors and LST

To gain more insights about the effects of urban density, vegetation cover, and water extents on LST in the study area, this research explored the correlation between these variables and the dependent LST variable. The analysis was based on splitting the area of interest into 31 grids as shown in **Figure 8**. The idea was to see the variations in these subareas and the correlation between the mean value of the variables and the mean LST. The results were represented as scatter plots. The summary statistics and a linear model were found between each independent variable and the LST. The analysis was carried our for three years, 2000, 2014, and 2018. Next sections explain the results of this analysis for each individual year.

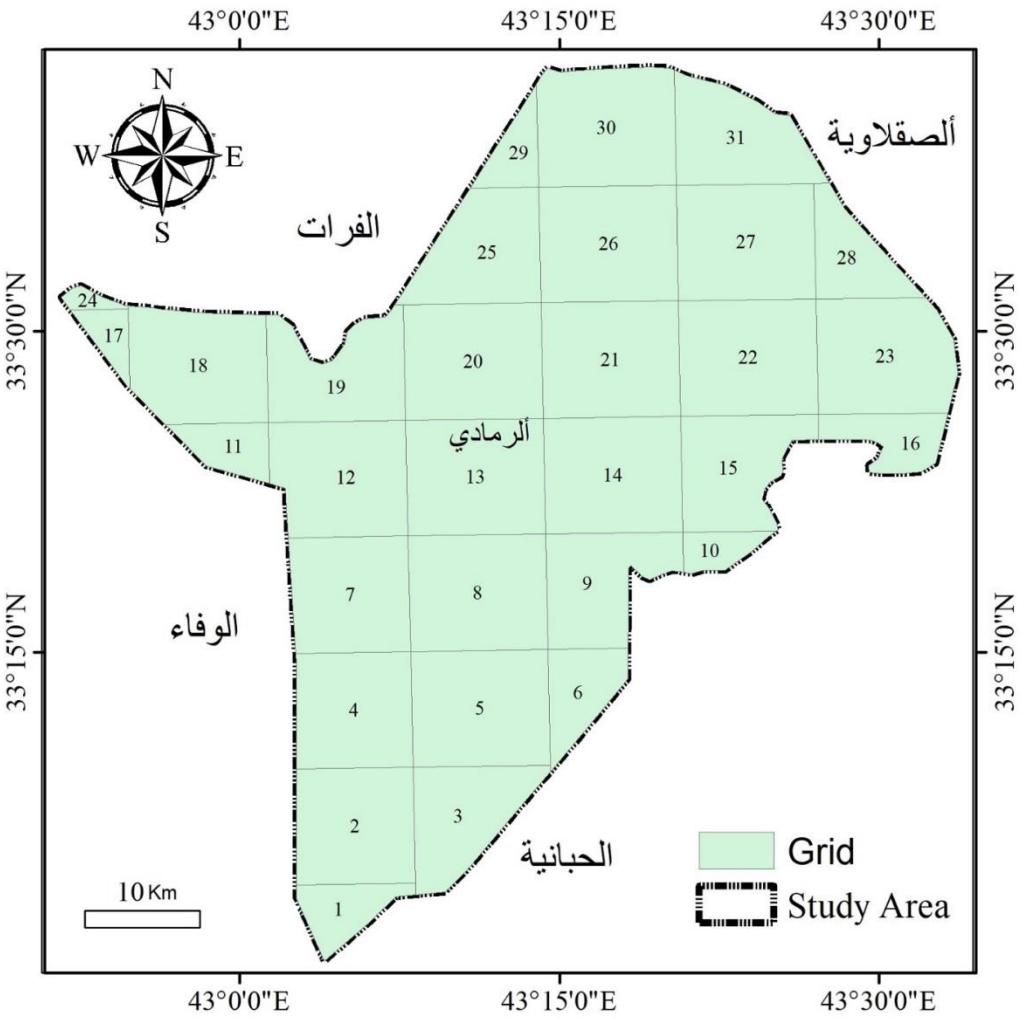

Figure 8: The study area divided into 31 grids.

3.5.1 Analysis of Year 2000

Figure 9 shows the scatter plots that visualize the correlations between NDBI, NDVI, and NDWI and LST for the year 2000. The results show positive correlations between NDBI and LST and NDWI and LST, whereas the correlation between NDVI and LST is negative. This means that the LST goes up when the area is denser and drier. In contrast, the areas with low NDVI values have high LST values. The correlation coefficient that was estimated between NDBI and LST is 0.70 which indicates a relatively strong correlation. The correlation coefficient between NDVI and LST was slightly lower, 0.67, whereas a low correlation of 0.34 was found between the NDWI and LST. The linear models can be used to predict LST from the given variables. This can be useful to project LST to the near future and take actions to control the environment and cool the heat in urban areas. The prediction from NDBI and NDVI will be more accurate than from NDWI, thus the first two variables are suggested to project LST in the study area based on this specific analysis.

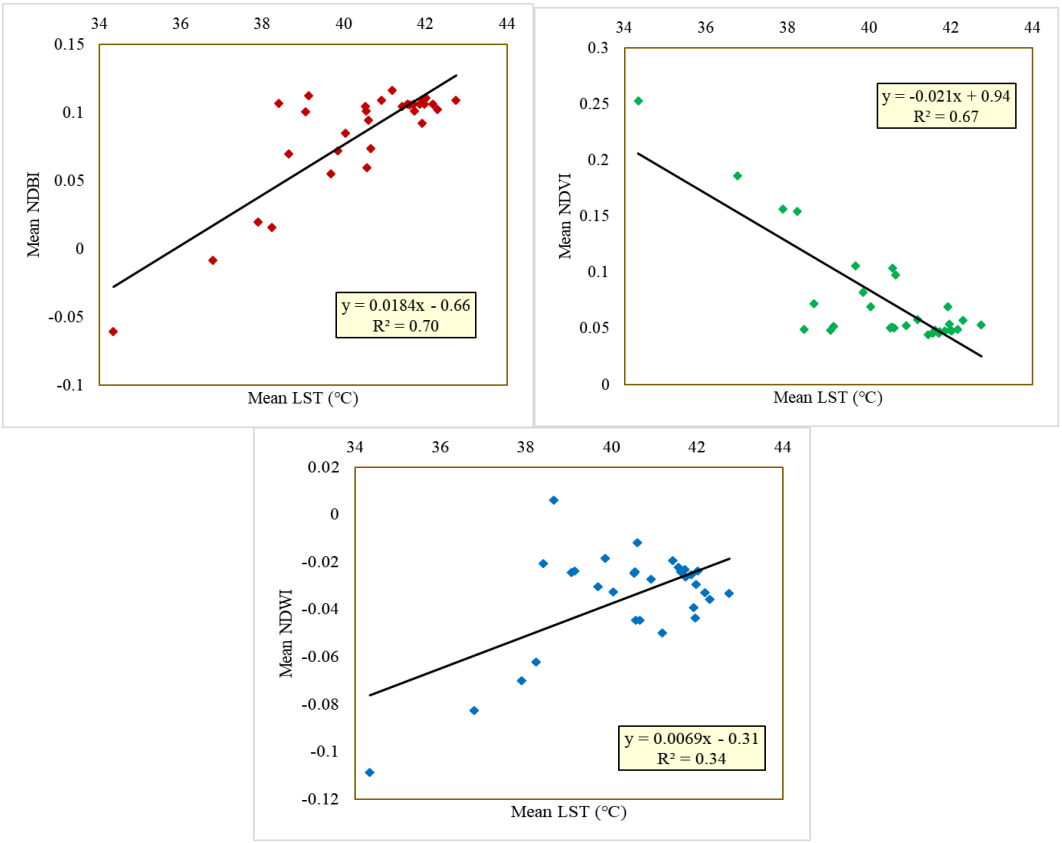

Figure 9: Scatter plots of the spectral indices (NDBI, NDVI, and NDWI) and LST over various regions in the study area (year 2000).

3.5.2 Analysis of Year 2014

The same correlation analysis was carried out for the year 2014 (**Figure 10**). The results show a different scenario, where there is a positive correlation only between NDBI and LST, and the correlations between NDVI and LST and NDWI and LST are negative. This is true because on this period the area witnessed less drought compared to the other dates. The correlation between the NDBI and LST is 0.75 which indicates a strong correlation. In fact, the correlation is higher by 0.05 compared to the earlier period, 2000. On the other hand, very weak correlation (0.0019) was found between NDVI and LST. This may be due to the outliers in the data. In addition, the correlation between NDWI and LST is 0.57, much higher than the correlation in the year 2000.

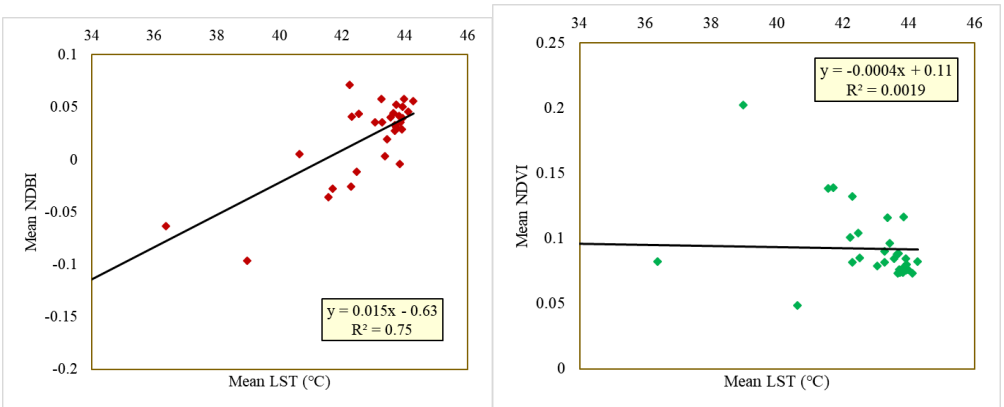

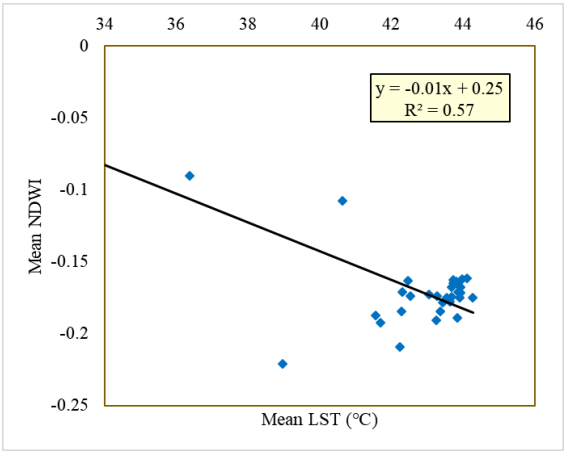

Figure 10: Scatter plots of the spectral indices (NDBI, NDVI, and NDWI) and LST over various regions in the study area (year 2014).

3.5.3 Analysis of Year 2018

The correlations between the spectral indices and LST in the most recent year (2018) are presented in **Figure 11**. The results suggest that there is relatively weak correlation between NDBI and LST (0.45), NDVI and LST (0.47) and NDWI and LST (0.27). These results show a positive correlation between NDBI and LST which was the case in the earlier periods, 2000 and 2014 as well. Moreover, negative correlations were found between NDVI and LST and NDWI and LST, also matches the results of the years 2000 and 2014.

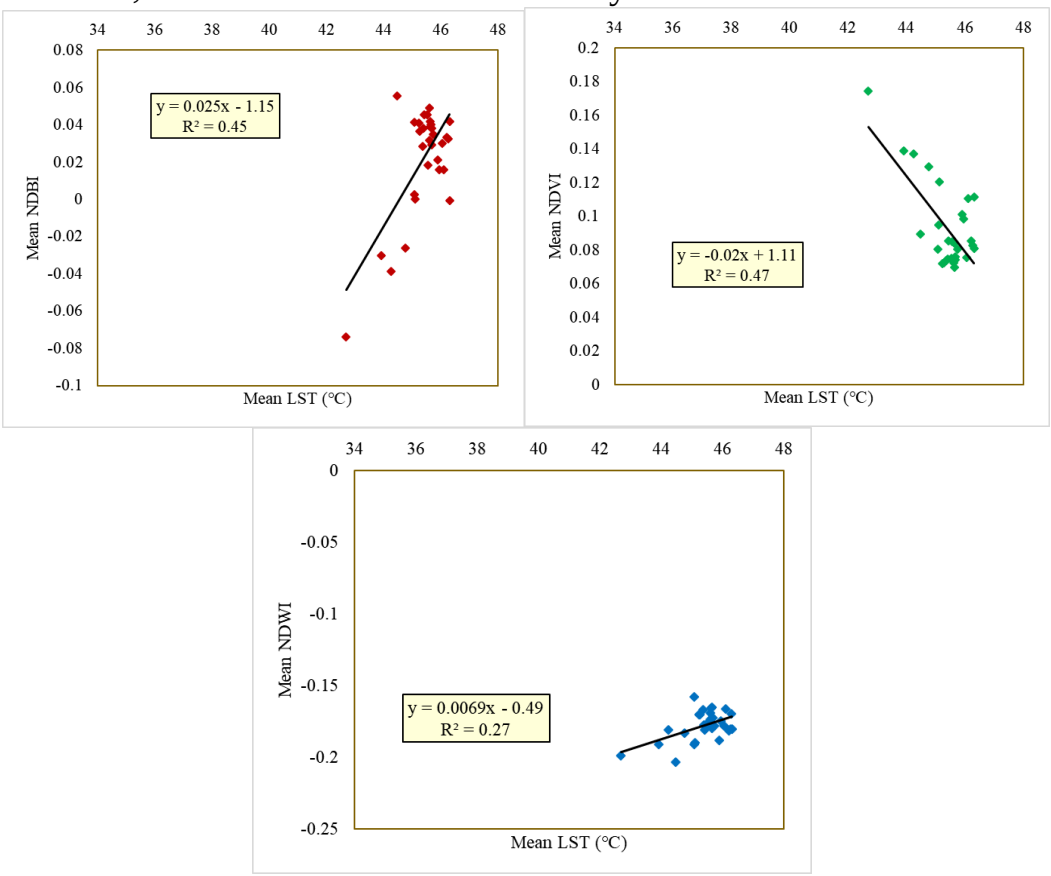

Figure 11: Scatter plots of the spectral indices (NDBI, NDVI, and NDWI) and LST over various regions in the study area (year 2018).

4. Conclusions

Thermal islands suggest that the land temperature in dense urban areas is often lower than in rural areas. There are many factors affecting the thermal islands including urban density, vegetation cover, and water body. This research explored the effects and the correlation of these variables calculated by three spectral indices namely NDBI, NDVI, and NDWI on the lands surface temperature. The findings suggested that the high temperature is correlated with the dense urban areas. The vegetation cover and water bodies contribute to lower the surface temperature in the areas of interest and the surroundings. This indicate that the decision makers should improve the green lands and artificial lakes to lower the surface temperature in dense and compact urban areas.

References

Alexander, P. J., O'Dwyer, B., Brennan, M., Mills, G., & Lynch, P. (2017). Land surface temperature climatology over urban surfaces: A blended approach. In *2017 Joint Urban Remote Sensing Event (JURSE)* (pp. 1–4). IEEE. doi:10.1109/JURSE.2017.7924599

Bernardo, N., Watanabe, F., Rodrigues, T., & Alcântara, E. (2017). Atmospheric correction issues for retrieving total suspended matter concentrations in inland waters using OLI/Landsat-8 image. *Advances in Space Research*, *59*(9), 2335–2348. doi:10.1016/j.asr.2017.02.017

Centre for Geoinformatics & Planetary Studies, Dept. of Geology, Periyar University, Salem, Tamilnadu, India, S., A., C.R., P., & Centre for Geoinformatics & Planetary Studies, Dept. of Geology, Periyar University, Salem, Tamilnadu, India. (2016). Statistical Correlation between Land Surface Temperature (LST) and Vegetation Index (NDVI) using Multi-Temporal Landsat TM Data. *International Journal of Advanced Earth Science and Engineering*, *5*(1), 333–346. doi:10.23953/cloud.ijaese.204

Comarazamy, D. E., Gonzalez, J. E., & Luvall, J. C. (2015). Quantification and mitigation of long-term impacts of urbanization and climate change in the tropical coastal city of San Juan, Puerto Rico. *International Journal of Low-Carbon Technologies*, *10*(1), 87–97. doi:10.1093/ijlct/ctt059

He, C., Gao, B., Huang, Q., Ma, Q., & Dou, Y. (2017). Environmental degradation in the urban areas of China: Evidence from multi-source remote sensing data. *Remote Sensing of Environment*, *193*, 65–75. doi:10.1016/j.rse.2017.02.027

Hilker, T. (2018). Surface reflectance/bidirectional reflectance distribution function. In *Comprehensive Remote Sensing* (Vol. 3, pp. 2–8). Elsevier. doi:10.1016/B978-0-12-409548-9.10347-1

Lavender, S., & Lavender, A. (2015). *Practical handbook of remote sensing*. CRC Press. doi:10.1201/b19044

Morrow, J. G., Huggins, D. R., & Reganold, J. P. (2017). Climate change predicted to negatively influence surface soil organic matter of dryland cropping systems in the inland pacific northwest, USA. *Frontiers in Ecology and Evolution*, *5*. doi:10.3389/fevo.2017.00010

Zhang, M., Bai, L., Wu, Z., & Gong, Y. (2016). Bidirectional reflection distribution function modeling of material surface in different temperature. In *2016 11th International Symposium on Antennas, Propagation and EM Theory (ISAPE)* (pp. 713–715). IEEE. doi:10.1109/ISAPE.2016.7834056

Zhu, Z., Woodcock, C. E., Holden, C., & Yang, Z. (2015). Generating synthetic Landsat images based on all available Landsat data: Predicting Landsat surface reflectance at any given time. *Remote Sensing of Environment*, *162*, 67–83. doi:10.1016/j.rse.2015.02.009